Chemistry–A European Journal
Research Article
doi.org/10.1002/chem.202201764
Chemistry Europe
European Chemical Societies Publishing
www.chemeurj.org

Intense Molar Circular Dichroism in Fully Conjugated All-Carbon Macrocyclic 1,3-Butadiyne Linked pseudo-*meta* [2.2]Paracyclophanes**

Eric Sidler,[a] Patrick Zwick,[a] Charlotte Kress,[a] Ksenia Reznikova,[a] Olaf Fuhr,[b] Dieter Fenske,[b] and Marcel Mayor*[a, b, c]

Abstract: The synthetic access to macrocyclic molecular topologies with interesting photophysical properties has greatly improved thanks to the successful implementation of organic and inorganic corner units. Based on recent reports, we realized that pseudo-*meta* [2.2]paracyclophanes (PCPs) might serve as optimal corner units for constructing 3D functional materials, owing to their efficient electronic communication, angled substituents and planar chirality. Herein, we report the synthesis, characterization and optical properties of four novel all-carbon enantiopure macrocycles bearing three to six pseudo-*meta* PCPs linked by 1,3-butadiyne units. The macrocycles were obtained by a single step from enantiopure, literature-known dialkyne pseudo-*meta* PCP and were unambiguously identified and characterized by state of the art spectroscopic methods and in part even by x-ray crystallography. By comparing the optical properties to relevant reference compounds, it is shown that the pseudo-*meta* PCP subunit effectively elongates the conjugated system throughout the macrocyclic backbone, such that already the smallest macrocycle consisting of only three subunits reaches a polymer-like conjugation length. Additionally, it is shown that the chiral pseudo-*meta* PCPs induce a remarkable chiroptical response in the respective macrocycles, reaching unprecedented high molar circular dichroism values for all-carbon macrocycles of up to 1307 $L\,mol^{-1}\,cm^{-1}$.

Introduction

The number of reports on carbon-based macrocyclic structures has seen a tremendous upward trend in recent years due to the promising photophysical properties and topological beauty such π-conjugated structures exhibit.[1–3] The access to these macrocycles has also greatly improved due to the development of new synthetic methodologies.[4–6] The necessity for strain-overcoming synthetic strategies becomes clear when considering the planar and linear conformation that *para*-substituted benzenes exhibit, which is the most prevalent building block in π-conjugated macrocycles. One of the most prominent macrocyclic structures featuring only *para*-benzene units is the cycloparaphenylene (CPP) with its radially oriented π surface, first synthesized in 2008 by Bertozzi and co-workers.[7] The synthesis of these strained CPPs was enabled by the ingenious implementation of angled cyclohexadiene corner units that facilitate macrocyclization reactions and are reductively aromatized in a final reaction step. Since then, many new synthetic strategies to overcome strain have been developed. These include for example the platinum (II) complex strategy,[8] the cyclohexane corner strategy,[9,10] the combination of Diels-Alder and retro-Diels-Alder reactions,[11] or the utilization of ethylene bridges,[12,13] which led to the synthesis of (gram scale) CPPs, zig-zag carbon nanobelts and cycloparaphenylene acetylenes (CPPAs). Apart from the predominant *para* substitution pattern, *meta*-substituted benzene units have also found their way into carbon-based materials. They were implemented as branching points for the construction of larger dendrimers,[14,15] as corner units for the formation of macrocycles,[16–21] or as general building blocks for polyarylenes.[22,23] Recently, they were also introduced into CPPs to enhance fluorescent properties.[24] While *meta*-substituted benzenes do provide an ideal angle enabling their strain-free integration in macrocyclic carbon-based topologies, the electronic communication between the substituents is limited due to cross-conjugation, making them less ideal for conjugated materials.[25,26]

[a] E. Sidler, Dr. P. Zwick, C. Kress, K. Reznikova, Prof. Dr. M. Mayor
Department of Chemistry
University of Basel
St. Johanns-Ring 19, 4056 Basel (Switzerland)
E-mail: marcel.mayor@unibas.ch

[b] Dr. O. Fuhr, Prof. Dr. D. Fenske, Prof. Dr. M. Mayor
Institute for Nanotechnology (INT)
Karlsruhe Institute of Technology (KIT)
P. O. Box 3640, 76021 Karlsruhe (Germany)

[c] Prof. Dr. M. Mayor
Lehn Institute of Functional Materials (LIFM)
School of Chemistry
Sun Yat-Sen University (SYSU)
510275 Guangzhou (P. R. China)

[**] A previous version of this manuscript has been deposited on a preprint server (https://doi.org/10.26434/chemrxiv-2022-79ct4-v2).

Supporting information for this article is available on the WWW under https://doi.org/10.1002/chem.202201764

[2.2]Paracyclophanes (PCPs) are moieties with two slightly bent face-to-face oriented benzene rings connected by two ethane bridges (Figure 1b). The different substitution patterns available in these structural units enable a large variety of distinct building blocks, making PCP a generally interesting subunit for 3D materials.[27] This is why PCPs are not unknown in the field of new functional materials. They have been used among other things for the construction of dendrimer structures,[28] macrocyclic metal complexes,[29] or one-handed double helices.[30] Recently, pseudo-*para* and pseudo-*meta* PCPs were also incorporated into CPPs[31,32] and a fourfold substituted PCP was used for helical chirality stabilization in oligothiophene macrocycles.[33] Triangle-shaped macrocycles consisting of pseudo-*ortho* PCPs with either *para*-phenylene-ethynylene or biphenyl linkers[34] were also reported, but their angle only allows the formation of limited ring sizes.[35,36]

In contrast to benzene, the electronic communication in pseudo-*para* and pseudo-*meta*-substituted PCPs is reversed. This was shown by Yoshizawa and co-workers, who theoretically predicted weak charge transport in pseudo-*para* and pseudo-*ortho* PCPs, and increased charge transport in pseudo-*meta* PCPs according to frontier orbital analysis.[37] Our group recently reported experimental evidence of destructive and constructive quantum interference (DQI and CQI) effects in pseudo-*para* and pseudo-*meta* substituted PCPs, respectively, thus corroborating the theoretical prediction.[38] With this finding, we figured that pseudo-*meta* PCPs might be ideal candidates for incorporation in π-conjugated materials. Unlike *para*-benzene, they combine optimal conjugation with an angled arrangement of the substituents, allowing construction of new types of topologies without the formation of excessive amounts of strain. Their angle facilitates macrocyclization, circumvents the need for specific corner units and their inherent chirality equips the materials with additional chiroptical properties. In this work, we thus show the synthesis, characterization and (chir)optical properties of four novel all-carbon macrocycles featuring several pseudo-*meta* PCP units connected by 1,3-butadiyne linkers. It is further demonstrated that the utilization of pseudo-*meta* PCP skips the need for corner units, enables conjugation throughout the macrocycles and induces a remarkable chiroptical response.

Results and Discussion

Design

We envisioned to synthesize the cyclized 1,3-butadiyne linked pseudo-*meta*-PCPs $(R_p)_n$-**1$_n$**, where n represents the number of pseudo-*meta*-PCP units, by a simple alkyne homocoupling of enantiopure dialkyne (R_p)-**S1**, resembling the recently reported chiral macrocyclic spirobifluorenes (Figure 2a).[39,40] The disconnection of the other enantiomers $(S_p)_n$-**1$_n$** can be performed analogously and leads to the enantiopure dialkyne (S_p)-**S1**.

Due to the fixed planar chirality of the enantiopure starting material, the formed macrocycles exhibit a formally interwoven pattern of helically arranged 1,4-diphenylbutadiyne connected by ethane bridges (Figure 2b) forming the PCP corner units. The dimensions of the formed interwoven polygon-shaped macrocycles are ultimately depending on the strain build-up in the ethane bridges and 1,3-butadiyne linkers, and the configurational stability of the pseudo-*meta*-PCP core. For reasons of simplicity, the synthesis and spectroscopic analysis are henceforth mainly discussed for the (R_p)-enantiomers, but were performed analogously for the (S_p)-enantiomers.

Synthesis and Characterization

To obtain the desired macrocyclic 1,3-butadiyne linked PCPs $(R_p)_n$-**1$_n$**, racemic dialkyne *rac*-**S1** was first synthesized according to literature procedures.[41] Unlike in the reported approach, the enantiomers were separated by chiral-phase high-performance liquid chromatography (HPLC) at the dialkyne stage in order to reduce the number of steps (Supporting Information Figure S8). In an initial macrocyclization attempt, subjecting the enantio-

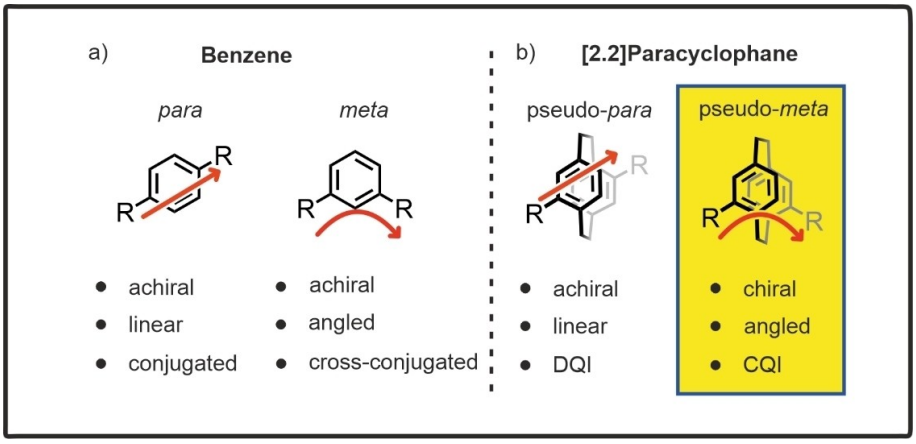

Figure 1. Comparison of chirality, directionality and electronics of a) *para*- and *meta*-substituted benzene, and b) pseudo-*para*- and pseudo-*meta*-substituted [2.2]paracyclophane.

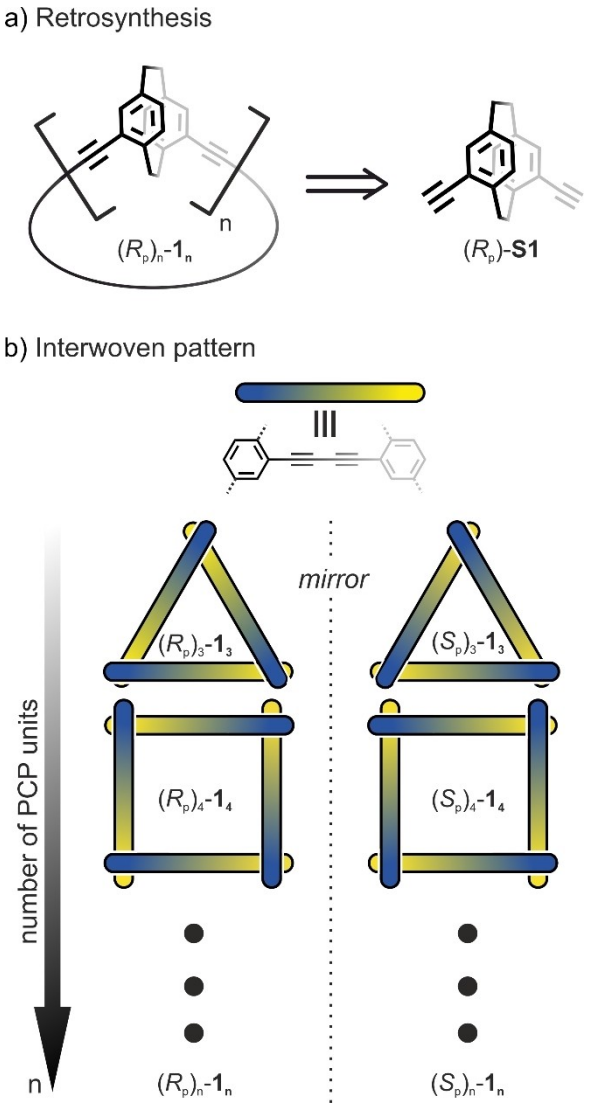

Figure 2. a) Retrosynthesis of the designed 1,3-butadiyne linked pseudo-*meta* PCPs (R_p)-$\mathbf{1}_n$, where n denotes the number of PCP units. Disconnection of the (S_p)-enantiomers can be done analogously, leading to (S_p)-**S1**. b) Illustration demonstrating the interwoven pattern of the macrocycles, emerging due to the fixed planar chirality of the PCP units. The interwoven blue/yellow rods can formally be seen as 1,4-diphenylbutadiyne linked by ethane bridges.

pure dialkyne (R_p)-**S1** to palladium-catalyzed Glaser coupling conditions at low concentration (1 mM) in toluene at 80 °C, gave a complex mixture of open-chain polymers and oligomers. Although only in very low amounts, desired macrocycles $(R_p)_3$-$\mathbf{1}_3$, $(R_p)_4$-$\mathbf{1}_4$ and $(R_p)_5$-$\mathbf{1}_5$ were identified by matrix-assisted laser desorption/ionization time-of-flight mass spectrometry (MALDI-ToF-MS).

When changing the conditions to a purely copper-mediated homocoupling using copper(I) chloride and copper(II) acetate in pyridine (1.5 mM, 84 mg scale) under inert atmosphere at 80 °C, the reaction proceeded much cleaner and the amount of open-chain oligomers and polymers was drastically reduced (Figure 3a). In the crude product, we observed the desired macrocycles bearing three to nine PCP units ($(R_p)_3$-$\mathbf{1}_3$ to $(R_p)_9$-$\mathbf{1}_9$) by MALDI-ToF-MS. While trimeric macrocycle $(R_p)_3$-$\mathbf{1}_3$ (29% yield) and tetrameric macrocycle $(R_p)_4$-$\mathbf{1}_4$ (20% yield) were readily purified by automated recycling gel permeation chromatography (GPC), pentameric macrocycle $(R_p)_5$-$\mathbf{1}_5$ (7% yield) and hexameric macrocycle $(R_p)_6$-$\mathbf{1}_6$ (1% yield) needed an additional purification step by normal-phase HPLC (Figure S30 and Figure S38). The amount of product of $(R_p)_7$-$\mathbf{1}_7$, $(R_p)_8$-$\mathbf{1}_8$, and $(R_p)_9$-$\mathbf{1}_9$ was too low for proper isolation and characterization. The identity of the macrocycles was corroborated by ^{1}H and ^{13}C{^{1}H} nuclear magnetic resonance (NMR) spectroscopy, and high-resolution MALDI-ToF-MS. The latter was instrumental to assign the dimensions of the macrocycles, which was further supported by their hydrodynamic radii deduced by the retention times in the GPC chromatogram (Figure S39). The high symmetry of all obtained macrocycles is reflected in the respective ^{1}H- and ^{13}C{^{1}H} NMR spectra, which show remarkable differences in chemical shifts compared to the starting material (R_p)-**S1** (see Figure 3b).

Comparing the ^{1}H NMR spectra of the starting material (R_p)-**S1** to those of the obtained macrocycles $(R_p)_3$-$\mathbf{1}_3$, $(R_p)_4$-$\mathbf{1}_4$, $(R_p)_5$-$\mathbf{1}_5$, and $(R_p)_6$-$\mathbf{1}_6$ in more detail (Figure 3b), the large differences in chemical shift of the ethane bridges ($H_{5a/b}$ and $H_{6a/b}$) become apparent. The signal of proton H_{6a}, which belongs to the inner ethane bridge of the PCP subunit in the macrocycles, is located at 3.49 ppm for (R_p)-**S1**. The signal shifts significantly downfield by 0.3 ppm to 3.79 ppm for $(R_p)_3$-$\mathbf{1}_3$. Upon increasing the ring size, the signal then gradually shifts upfield to 3.69 ppm for $(R_p)_6$-$\mathbf{1}_6$. Proton H_{6b}, which is connected to the same carbon atom as H_{6a} and thus also part of the inner ethane bridge of the PCP subunit, is part of the same multiplet as outer ethane proton H_{5b} of (R_p)-**S1**, residing at 3.08 ppm. For the macrocycles, however, the signals shift similarly as for H_{6a}. After a strong downfield shift of 0.34 ppm for $(R_p)_3$-$\mathbf{1}_3$, the signal receives an upfield shift when increasing the ring size, reaching 3.25 ppm for $(R_p)_6$-$\mathbf{1}_6$. An almost identical trend is observed for outer ethane bridge proton H_{5b}, which is now clearly separated from H_{6b}. The second proton of the outer ethane bridge, H_{5b}, is behaving rather differently, as it is upfield shifted by 0.12 and 0.04 ppm for $(R_p)_3$-$\mathbf{1}_3$ and $(R_p)_4$-$\mathbf{1}_4$, respectively, but displays hardly any shift for pentameric macrocycle $(R_p)_5$-$\mathbf{1}_5$ and only a small downfield shift of 0.03 ppm for $(R_p)_6$-$\mathbf{1}_6$ compared to (R_p)-**S1**. Concerning the aromatic protons, the shifts tend to be less pronounced than for the ethane bridge protons. The doublet of proton H_3, which is at 7.00 ppm for (R_p)-**S1**, shifts downfield to 7.09 and 7.10 for $(R_p)_3$-$\mathbf{1}_3$ and $(R_p)_4$-$\mathbf{1}_4$, but then shifts only marginally for $(R_p)_5$-$\mathbf{1}_5$ and $(R_p)_6$-$\mathbf{1}_6$. Doublet of doublets of H_2 shifts from 6.49 ppm to 6.58 ppm for $(R_p)_3$-$\mathbf{1}_3$, but then stays comparable for the larger ring sizes. Lastly, proton H_1 receives a small upfield shift of 0.01 ppm for trimer $(R_p)_3$-$\mathbf{1}_3$, followed by a gradual downfield shift up to 6.69 ppm for $(R_p)_6$-$\mathbf{1}_6$.

Generally, no structure-related apparent rationale can be concluded from the chemical shifts of the individual protons. However, the largest differences in chemical shifts were observed for trimeric $(R_p)_3$-$\mathbf{1}_3$, attributed to the higher strain in the macrocycle, leading to a more pronounced geometric distortion compared to the other compounds. We further noted

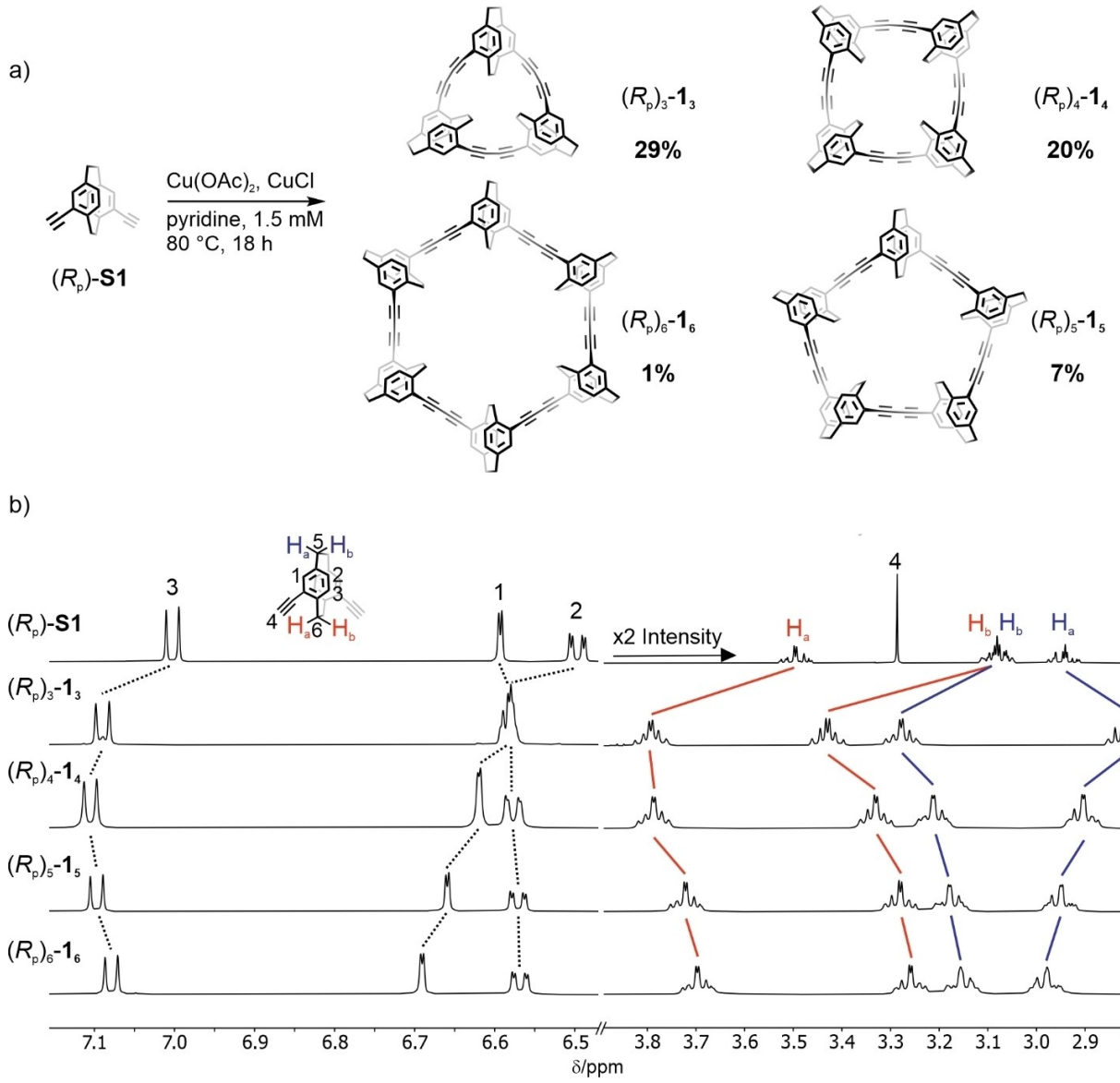

Figure 3. a) Synthetic scheme towards isolated $(R_p)_3$-**1**$_3$, $(R_p)_4$-**1**$_4$, $(R_p)_5$-**1**$_5$, and $(R_p)_6$-**1**$_6$. Synthesis of the (S_p) enantiomers was performed analogously. b) Comparison of the ^{1}H NMR spectra (500 MHz, $CDCl_3$, 298 K) of $(R_p)_3$-**1**$_3$, $(R_p)_4$-**1**$_4$, $(R_p)_5$-**1**$_5$, and $(R_p)_6$-**1**$_6$. For a better visibility, the intensity was doubled for the high field proton resonances. The NMR spectra of the (S_p)-enantiomers are identical to those of the (R_p)-enantiomers.

that the signals of the ethane bridge protons tend to shift towards the frequencies of the starting material (R_p)-**S1** upon increasing the ring size, which might indicate more relaxed geometries of the PCP units in the larger macrocycles. Also, the individual shifts of the ethane bridge protons indicate no presence of global aromatic or antiaromatic ring current in the neutral macrocycles. This behaviour might be different in oxidized or reduced species, which is under current investigation. The $^{13}C\{^1H\}$ NMR spectra show 10 signals for each of the compounds, being consistent with the expected high symmetry of the obtained structures (Figures S2, S10, S17, S24, and S32).

Needle-like single crystals suitable for x-ray diffraction experiments were obtained by slow diffusion of acetonitrile vapours into a solution of $(R_p)_4$-**1**$_4$ in chloroform. The solid-state structure and packing of $(R_p)_4$-**1**$_4$ are displayed in Figure 4. The compound crystallized in the space group $P2_1$ containing two molecules in the unit cell (Figure S53). In the solid state, $(R_p)_4$-**1**$_4$ adopts a noticeable rectangular shape with two shorter 1,3-butadiynes of 6.49 Å (Figure 4a, red interspace) and two longer ones (blue interspace) of 6.66 and 6.64 Å. Consequently, the shorter 1,3-butadiyne units bear more bent triple carbon-carbon bonds with angles of 169.2° and 169.5°, and more straight triple bonds with angles of 176.5° and 179.3° in the longer 1,3-butadiyne units. In the side view, the slope of the 1,3-butadiyne unit relative to the lower benzenes of two connected PCP cores of 19.1° and thus the interwoven pattern becomes apparent. Similar to some CPPs,[42] $(R_p)_4$-**1**$_4$ adopts a herringbone-type packing that leads to a tubular arrangement of the individual

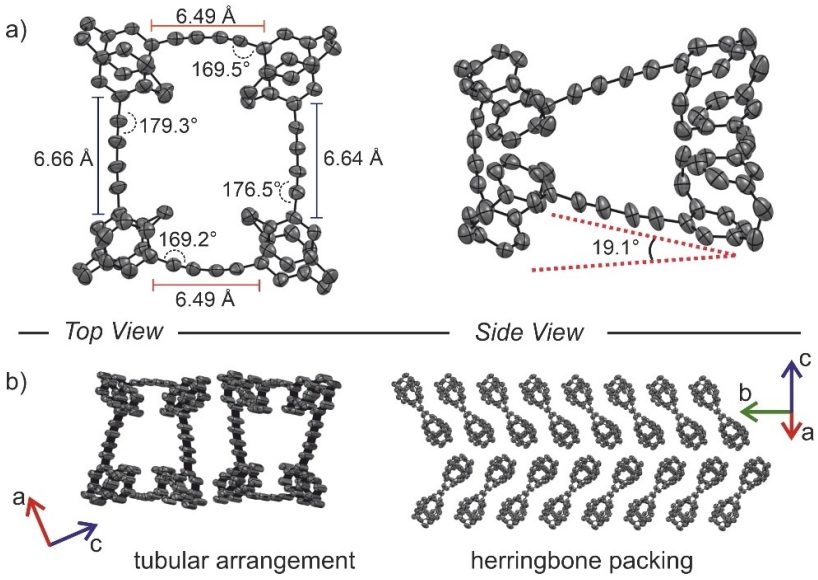

Figure 4. Top and side view Oak Ridge Thermal Ellipsoid plots (ORTEP) of the solid state structure of $(R_p)_4$-**1**$_4$ (a) and its packing (b). Hydrogen atoms and solvent molecules are omitted for clarity. Thermal ellipsoids are plotted on a 50% probability level.

macrocycles when changing to the top view along the b-axis (Figure 4b). Numerous attempts to grow suitable crystals for trimeric, pentameric, and hexameric macrocycles were not successful so far.

Optical Properties

The absorption and emission spectra of the dialkyne (R_p)-**S1** are compared to the obtained macrocycles (left side of Figure 5). The highest wavelength transition (λ_{max}) of (R_p)-**S1** lies at 285 nm with a molar absorption coefficient (ε) of 9308 L mol^{-1} cm^{-1}. The measured emission peak has its maximum at 382 nm, resulting in a large *Stokes* shift of 97 nm. On the other hand, trimeric macrocycle $(R_p)_3$-**1**$_3$ displays two main absorption bands at 331 and 369 nm (λ_{max}) with ε = 66486 and 45911 L mol^{-1} cm^{-1}, respectively. Likewise, the normalized emission spectrum features two main bands at 385 nm and 418 nm, resulting in a quite small *Stokes* shift of 16 nm. The much smaller *Stokes* shift is unsurprising, given the expected increased rigidity of the macrocycle as compared to the dialkyne (R_p)-**S1**. The two main absorption bands of $(R_p)_4$-**1**$_4$ lie at 340 (ε = 118982 L mol^{-1} cm^{-1}) and 370 nm (λ_{max}, ε = 106275 L mol^{-1} cm^{-1}), showing a massive non-linear increase of the molar absorption coefficient. The same transitions for pentameric macrocycle $(R_p)_5$-**1**$_5$ lie at 341 (ε = 133059 L mol^{-1} cm^{-1}) and 370 nm (λ_{max}, ε = 134695 L mol^{-1} cm^{-1}), showcasing a less noteworthy increase of the molar absorption coefficient. The absorption of hexameric $(R_p)_6$-**1**$_6$ for both transitions is fairly comparable to the pentameric macrocycle with energies at 342 (ε = 130646 L mol^{-1} cm^{-1}) and 370 nm (λ_{max}, ε = 137382 L mol^{-1} cm^{-1}). Notably, the energy of the transition at λ_{max} changes insignificantly with increasing ring size and converges to 370 nm. Likewise, the normalized emission spectra are similar for all four macrocycles. These two observations show that the effective conjugation length remains the same in all macrocyclic model compounds, pointing at the exceptional conjugation within the obtained macrocycles (see section Conjugated System).

The aforementioned non-linear increase of the absorption coefficient is displayed in the left graph of Figure 5c, where the $\varepsilon(\lambda_{max})$ values are plotted against the number of PCP subunits and compared to a hypothetical linear increase extrapolated from the values of trimeric macrocycle $(R_p)_3$-**1**$_3$ (solid line). The increase is most intense when going from trimeric to tetrameric macrocycle, where the intensity increases by 2.3 times, although the number of PCP subunits increases just times 1.33. Upon increasing the ring size, the non-linear effect decreases, and the absorption coefficient seems to increase much less with the number of PCP units. To confirm whether the oscillator strengths indeed adhere to a seemingly hyperbolic behaviour regarding the number of PCP subunits, larger ring sizes are in need.

In the circular dichroism (CD) spectra (Figure 5a, right side), dialkyne (R_p)-**S1** shows three main Cotton bands at 287, 262 and 244 nm with moderate molar circular dichroism values ($\Delta\varepsilon$) of −94, 52 and 135 L mol^{-1} cm^{-1}, respectively. Compared to that, trimeric macrocycle $(R_p)_3$-**1**$_3$ shows two main Cotton bands at 349 and 377 nm with strong molar circular dichroism values of −218 and −523 L mol^{-1} cm^{-1}. Similar to the absorption spectra, the main peaks in the CD spectra do hardly shift in energy when increasing the ring size, but the molar circular dichroism values vary drastically. The Cotton bands of $(R_p)_4$-14 show particularly strong molar circular dichroism values of up to −1186 L mol^{-1} cm^{-1} for the transition at 377 nm and $(R_p)_5$-**1**$_5$ shows even higher values of −1247 L mol^{-1} cm^{-1} (+1307 L mol^{-1} cm^{-1} for $(S_p)_5$-**1**$_5$). To the best of our knowledge,

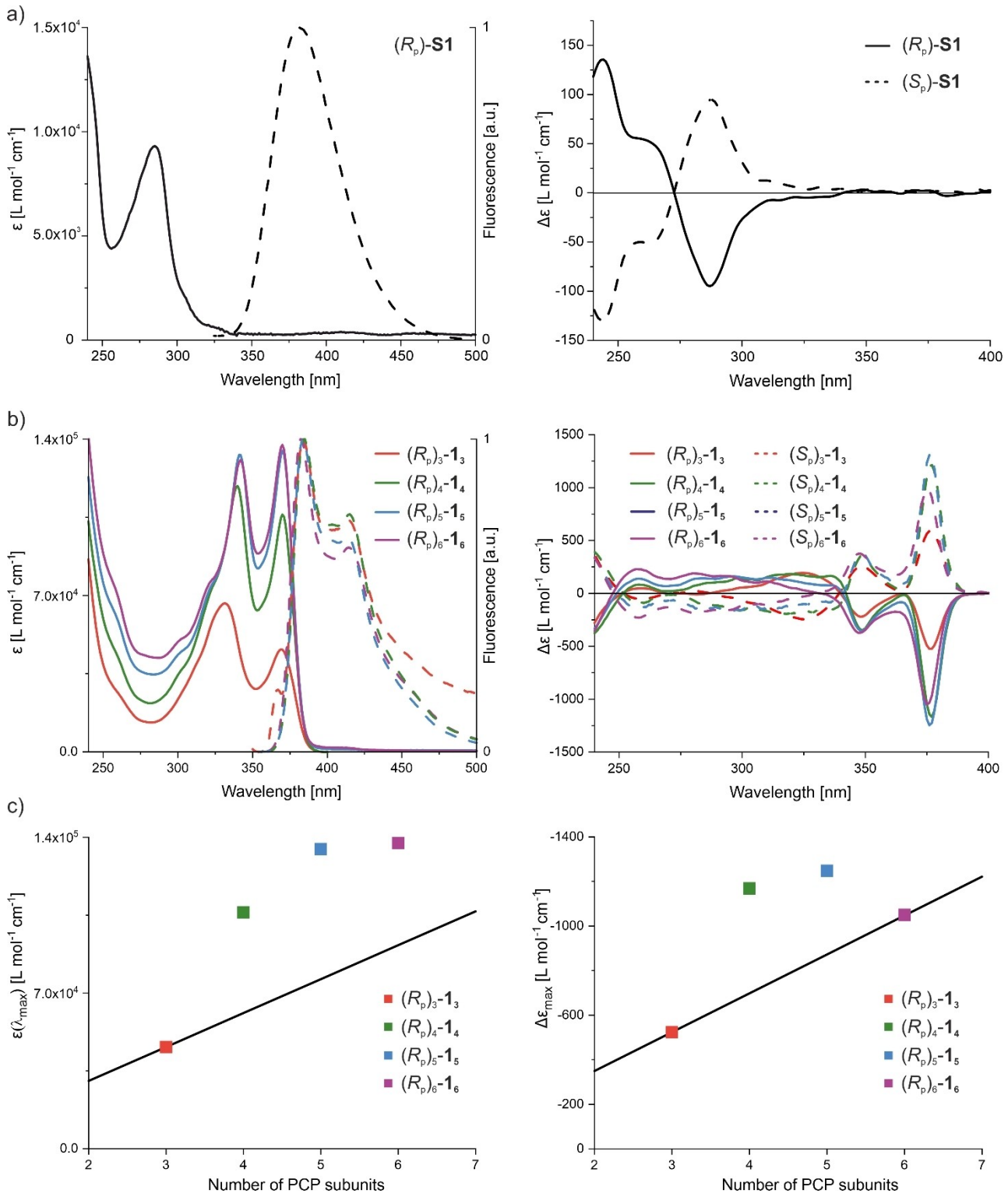

Figure 5. a) Left: Absorption (solid line) and emission (dashed line, excitation at 285 nm) spectra of (R_p)-**S1** in CH_2Cl_2 (c ~ 10^{-6} M). Right: Circular dichroism spectra of (R_p)-**S1** (solid line) and (S_p)-**S1** (dashed line) in CH_2Cl_2 (c ~ 10^{-6} M). b) Left: Absorption (solid line) and emission (dashed line) spectra of $(R_p)_3$-$\mathbf{1}_3$ (red), $(R_p)_4$-$\mathbf{1}_4$ (green), $(R_p)_5$-$\mathbf{1}_5$ (blue), and $(R_p)_6$-$\mathbf{1}_6$ (purple) in CH_2Cl_2 (c ~ 10^{-6} M). Compounds $(R_p)_3$-$\mathbf{1}_3$, $(R_p)_4$-$\mathbf{1}_4$, $(R_p)_5$-$\mathbf{1}_5$, and $(R_p)_6$-$\mathbf{1}_6$ were excited at 330, 340, 340, and 340 nm, respectively. Absorption and emission spectra were comparable for the (S_p)-enantiomers. Right: Circular dichroism spectra of the (R_p)-enantiomers (solid line) and (S_p)-enantiomers (dashed line) of $\mathbf{1}_3$ (red), $\mathbf{1}_4$ (green), $\mathbf{1}_5$ (blue) and $\mathbf{1}_6$ (purple) in CH_2Cl_2 (c ~ 10^{-6} M). c) Left: $\varepsilon(\lambda_{max})$ values of $(R_p)_3$-$\mathbf{1}_3$ (red), $(R_p)_4$-$\mathbf{1}_4$ (green), $(R_p)_5$-$\mathbf{1}_5$ (blue), and $(R_p)_6$-$\mathbf{1}_6$ (purple) are plotted versus the number of PCP subunits and compared to a hypothetical linear relationship extrapolated from the values of $(R_p)_3$-$\mathbf{1}_3$ (solid line). Right: $\Delta\varepsilon_{max}$ values of $(R_p)_3$-$\mathbf{1}_3$ (red), $(R_p)_4$-$\mathbf{1}_4$ (green), $(R_p)_5$-$\mathbf{1}_5$ (blue), and $(R_p)_6$-$\mathbf{1}_6$ (purple) are plotted versus the number of PCP subunits and compared to a hypothetical linear relationship extrapolated from the values of $(R_p)_3$-$\mathbf{1}_3$ (solid line).

this is the most intense molar circular dichroism value for macrocyclic all-carbon molecules reported to date, surpassing those of alleno-acetylenic macrocycles[43] and also those of helicene oligomers.[44] Strikingly, the intensity of the Cotton effect of hexameric macrocycle $(R_p)_6$-**1**$_6$ drops to 1049 L mol^{-1} cm^{-1} and is thus even lower than for $(R_p)_4$-**1**$_4$. Hence, when plotting the $\Delta\varepsilon_{max}$ values against the number of PCP subunits and compare it to a linear relationship obtained by extrapolating the values of $(R_p)_3$-**1**$_3$, no hyperbolic behaviour is observed. The Cotton effect first increases 2.3 times for $(R_p)_4$-**1**$_4$, identically to the absorption spectra, followed by only a very minor increase for $(R_p)_5$-**1**$_5$, and a strong drop for $(R_p)_6$-**1**$_6$, which noteworthy matches the value of the before mentioned linear relationship. However, this behaviour might be coincidental. The relatively low molar circular dichroism value of $(R_p)_6$-**1**$_6$ can be attributed to an increase in conformational degrees of freedom. While the angle of 120° between *meta* substituents in benzene is ideal for the formation of a hexagon,[45] pseudo-*meta* substituents tend to have a varying angle due to the favoured bent and distorted conformation and the off-set twisting of the benzenes in the PCP core.[46] This presumably leads to a larger variety of conformations and thus a decreased rigidity, which is known to influence the chiroptical response.[47,48] The main values of the photophysical analysis are summarized in Table 1. To rule out potential aggregation and to determine more exact extinction coefficients and molar circular dichroism values, dilution series of the macrocycles were measured (Figures S44–S51).

In order to get an understanding of the origin of the intense chiroptical response that the macrocycles display, g-factor plots were analyzed. The g-factor, which is also known as the anisotropy or dissymmetry factor, is defined as the ratio of molar circular dichroism and molar absorption ($\Delta\varepsilon/\varepsilon$) and provides information about the magnetic contribution to a given Cotton effect.[49] The plot shows fairly high g-factor values, reaching up to 0.024 for $(R_p)_4$-**1**$_4$ (Figure S52), however, there are only minor differences between the g-factor plots of the individual macrocycles. The large differences in Cotton effect intensities can thus not be explained by a magnetic contribution to the transition but is rather originating from an increase in contribution of the electronic transition dipole moment, which is consistent with the strong molar absorption values observed.

Table 1. Comparison of the main absorption, emission and circular dichroism values of (R_p)-**S1**, $(R_p)_3$-**1**$_3$, $(R_p)_4$-**1**$_4$, $(R_p)_5$-**1**$_5$, and $(R_p)_6$-**1**$_6$.

Comp.	λ_{max} [nm]	$\varepsilon_{\lambda max}$ [L mol^{-1} cm^{-1}]	λ_{em} (excitation) [nm]	$\Delta\varepsilon_{max}$ [L mol^{-1} cm^{-1}][a]
(R_p)-**S1**	285	9308	382 (285)	135 (−129)
$(R_p)_3$-**1**$_3$	369	45911	385, 418 (330)	−523 (+587)
$(R_p)_4$-**1**$_4$	370	106275	385, 418 (340)	−1186 (+1213)
$(R_p)_5$-**1**$_5$	370	134695	385, 418 (340)	−1247 (+1307)
$(R_p)_5$-**1**$_6$	370	137382	385, 418 (340)	−1049 (+988)

[a] values of the (S_p)-enantiomers are in brackets.

Conjugated System

When comparing conjugated systems with similar substituents, a redshift in the absorption spectra is associated with an increase in conjugation length. Given the observation that the highest wavelength transition λ_{max} in the absorption spectrum converges to 370 nm upon enlarging the ring size, the question arises whether the conjugation pathways are interrupted, or if the system is conjugated effectively. To investigate this matter, commercially available compound **2** and literature known molecule **3**[50] were identified as relevant reference compounds (Figure 6a). Namely, 1,4-diphenylbutadiyne (**2**) would make up the simplest conjugated subsystem of the macrocycles if no coupling through the PCP core existed. On the other hand, compound **3** would manifest the smallest subsystem if conjugation is interrupted beyond one PCP core. The absorption spectra of the reference compounds are compared to the trimeric $(R_p)_3$-**1**$_3$ in Figure 6b. The highest wavelength transition

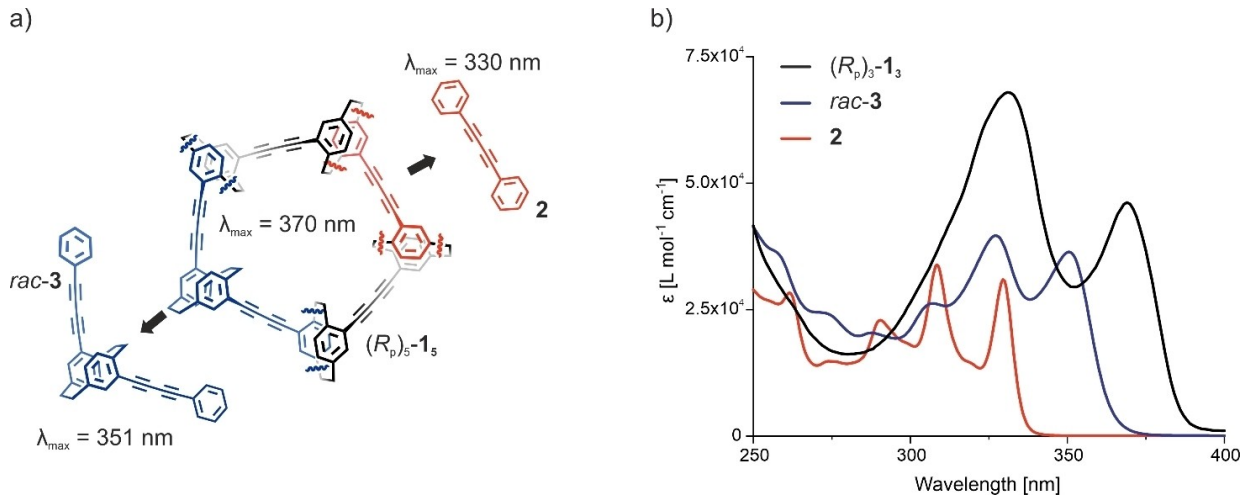

Figure 6. a) Reference compounds **2** and **3**, which manifest small sub-segments of the macrocycles, are displayed together with their highest wavelength transition λ_{max}. b) Absorption spectra of **2** (red), *rac*-**3** (blue) and $(R_p)_3$-**1**$_3$ (black) in CH_2Cl_2 (c ~ 10^{-6} M).

λ_{max} for **2** lies at 330 nm, which is redshifted by 21 nm to 351 nm for reference compound **3**. This observation suggests efficient conjugation through the pseudo-*meta* PCP moiety. Taking into account that λ_{max} for $(R_p)_3$-**1$_3$** is further redshifted by 18 nm to 369 nm as compared to **3** and that λ_{max} converges to 370 nm when increasing the ring size, it was concluded that the conjugated system is extended beyond one PCP core and that it is efficiently conjugated throughout the whole macrocyclic backbone. This conclusion is further supported by the absorption spectra of fast eluting bands in the GPC chromatogram (Figures S40–S43), when employing the initial reaction conditions mainly producing open-chain polymers and oligomers. The absorption spectra of these fast-eluting compounds display a near identical shape as the macrocycles $(R_p)_3$-**1$_3$**, $(R_p)_4$-**1$_4$**, $(R_p)_5$-**1$_5$**, and $(R_p)_6$-**1$_6$**, and their λ_{max} is converging from 368 nm toward 370 nm. This finding suggests that these macrocycles are so efficiently conjugated that they obtain an astonishing polymer-like conjugation length despite their rather small size.

Conclusion

It could be shown that the angle offered by pseudo-*meta* substituted PCPs allows to construct trimeric, tetrameric, pentameric, and hexameric 1,3-butadiyne linked macrocycles $(R_p)_3$-**1$_3$**, $(R_p)_4$-**1$_4$**, $(R_p)_5$-**1$_5$**, and $(R_p)_6$-**1$_6$**, respectively, in remarkably high yields. The electronic through-space communication of the pseudo-*meta* PCPs evidently leads to a thoroughly conjugated system, yielding polymer-like states already for the smallest of the macrocycles in the studied series. The molar absorption coefficient appears to follow a hyperbolic behavior regarding the number of PCP units, and the inherent chirality of the pseudo-*meta* PCPs leads to a strong chiroptical response with unrivalled molar circular dichroism values for all-carbon macrocycles of up to 1307 $L\,mol^{-1}\,cm^{-1}$ for $(S_p)_5$-**1$_5$**. These findings prove pseudo-*meta* PCP to be a viable corner unit for the construction of various 3D functional materials, and suggest efficient incorporation into π-conjugated material that would otherwise suffer from unfavourable strain energies. We are currently looking into density-functional theory (DFT) calculations to get a deeper understanding of the origin of the intense chiroptical response, and plan to investigate the circularly polarized luminescence (CPL) and global (anti)aromatic character of the obtained macrocycles.

Experimental Section

Complete experimental details and characterization data, NMR spectra, mass spectra, HPLC chromatograms, GPC chromatograms, UV-Vis spectra, g-factor plot, and crystallographic data can be found in the Supporting Information.

Synthesis of $(S_p)_3$-**1$_3$**, $(S_p)_4$-**1$_4$**, $(S_p)_5$-**1$_5$**, and $(S_p)_6$-**1$_6$**

Preparation of reagents: CuCl (15 g) was purified by washing it with aqueous HCl (1 M) and drying it under vacuum. $Cu(OAc)_2$ (10 g) was purified by refluxing in Ac_2O (50 mL) overnight, filtering it under N_2, washing with THF and drying under vacuum.

Synthetic Procedure: A dry two-neck round-bottom flask was charged with dry pyridine (165 mL), CuCl (583 mg, 5.89 mmol, 18 equiv.) and $Cu(OAc)_2$ (1.663 g, 9.16 mmol, 28 equiv.). The solution was degassed by purging with argon for 1 h and heated to 80 °C. (S_p)-**S1** (84 mg, 327 μmol, 1 equiv.) was dissolved in pyridine (55 mL), degassed by purging with argon for 1 h and added dropwise with a dropping funnel to the previously prepared solution. After 18 h the reaction mixture was allowed to cool down to room temperature and the solvent was removed under vacuum. The solid residue was redissolved in CH_2Cl_2, washed with HCl (1 M, 2×) and brine, and dried over anhydrous Na_2SO_4. After removing the solvent under vacuum, the residue was purified by flash column chromatography (SiO_2, cyclohexane/toluene/ethylacetate, 15:2:1) and the combined fractions comprising the macrocyclic products were concentrated and subjected to automated recycling gel-permeation chromatography (GPC), where analytically pure $(S_p)_3$-**1$_3$** (24 mg, 29%) and $(S_p)_4$-**1$_4$** (17 mg, 20%) were isolated as the slowest and second slowest eluting band, respectively. The third and fourth eluting band were each concentrated and subjected to normal-phase HPLC to give $(S_p)_5$-**1$_5$** (6 mg, 7%) and $(S_p)_6$-**1$_6$** (1 mg, 1%), respectively. All macrocycles were isolated as white solids.

The synthesis of the (R_p)-enantiomers was performed identically, and the analytical data matched the data of the (S_p)-enantiomers.

Analytical data of $(S_p)_3$-1$_3$: R_f = 0.71 (cyclohexane/toluene/ethylacetate (15:2:1)); m.p. > 350 °C; ^{1}H NMR (600 MHz, $CDCl_3$, 298 K): δ = 7.09 (d, J = 8.4 Hz, 1H), 6.65–6.54 (m, 2H), 3.83–3.75 (m, 1H), 3.47–3.39 (m, 1H), 3.30–3.25 (m, 1H), 2.86–2.78 ppm (m, 1H); ^{13}C{^{1}H} NMR (151 MHz, $CDCl_3$, 298 K): δ = 146.52, 139.98, 133.87, 133.00, 131.79, 123.74, 88.19, 80.69, 35.31, 34.35 ppm; HR-MS (MALDI-ToF, +): *m/z* calcd. for $C_{60}H_{42}Ag$ $[M+Ag]^+$: 869.2332, found: 869.2342.

Analytical data of $(S_p)_4$-1$_4$: R_f = 0.60 ((cyclohexane/toluene/ethylacetate (15:2:1)); m.p. > 350 °C; ^{1}H NMR (500 MHz, $CDCl_3$, 298 K): δ = 7.10 (d, J = 7.8 Hz, 1H), 6.62 (d, J = 1.9 Hz, 1H), 6.58 (dd, J = 7.9, 1.9 Hz, 1H), 3.84–3.74 (m, 1H), 3.38–3.28 (m, 1H), 3.26–3.16 (m, 1H), 2.96–2.85 ppm (m, 1H); ^{13}C{^{1}H} NMR (126 MHz, $CDCl_3$, 298 K): δ = 145.46, 139.90, 135.74, 133.03, 131.46, 124.02, 84.15, 78.83, 35.13, 33.82 ppm; HR-MS (MALDI-ToF, +): *m/z* calcd. for $C_{80}H_{56}Ag$ $[M+Ag]^+$: 1123.3427, found: 1123.3447.

Analytical data of $(S_p)_5$-1$_5$: R_f = 0.45 ((cyclohexane/toluene/ethylacetate (15:2:1)); m.p. > 350 °C; ^{1}H NMR (600 MHz, $CDCl_3$, 298 K): δ = 7.10 (d, J = 7.8 Hz, 1H), 6.66 (d, J = 1.9 Hz, 1H), 6.57 (dd, J = 7.9, 1.9 Hz, 1H), 3.76–3.68 (m, 1H), 3.33–3.24 (m, 1H), 3.22–3.12 (m, 1H), 2.99–2.91 ppm (m, 1H); ^{13}C{^{1}H} NMR (151 MHz, $CDCl_3$, 298 K): δ = 144.66, 139.90, 136.80, 133.15, 131.37, 124.09, 82.88, 78.10, 35.06, 33.49 ppm; HR-MS (MALDI-ToF, +): *m/z* calcd. for $C_{100}H_{70}Ag$ $[M+Ag]^+$: 1377.4523, found: 1377.4546.

Analytical data of $(S_p)_6$-1$_6$: R_f = 0.33 ((cyclohexane/toluene/ethylacetate (15:2:1)); m.p. > 350 °C; ^{1}H NMR (600 MHz, $CDCl_3$, 298 K): δ = 7.08 (d, J = 7.8 Hz, 1H), 6.69 (d, J = 1.9 Hz, 1H), 6.57 (dd, J = 7.9, 1.9 Hz, 1H), 3.74–3.65 (m, 1H), 3.30–3.23 (m, 1H), 3.20–3.12 (m, 1H), 3.02–2.93 ppm (m, 1H); ^{13}C{^{1}H} NMR (151 MHz, $CDCl_3$, 298 K): δ = 144.25, 139.91, 137.37, 133.27, 131.37, 124.17, 82.64, 77.83, 35.06, 33.45 ppm; HR-MS (MALDI-ToF, +): *m/z* calcd. for $C_{120}H_{84}$ $[M]^+$: 1524.6568, found: 1524.6567.

Deposition Number 2172361 contains the supplementary crystallographic data for this paper. These data are provided free of charge by the joint Cambridge Crystallographic Data Centre and Fachinformationszentrum Karlsruhe Access Structures service.

Acknowledgements

The authors acknowledge generous financial support by the Swiss National Science Foundation (SNF grant number 200020-207744) and by the 111 project (90002-18011002). The study was further partially funded by the FET open project QuIET (no. 767187). The authors thank Pascal Rieder for support with the cryo NMR. Open access funding provided by Universität Basel. Open Access funding provided by Universität Basel.

Conflict of Interest

The authors declare no conflict of interest.

Data Availability Statement

The data that support the findings of this study are available in the supplementary material of this article.

Keywords: [2.2]paracyclophane · hydrocarbon · macrocycle · molar circular dichroism · π-conjugation

[1] Y. Xu, M. Delius, *Angew. Chem. Int. Ed.* **2020**, *59*, 559–573; *Angew. Chem.* **2020**, *132*, 567–582.
[2] M. Hasegawa, Y. Nojima, Y. Mazaki, *ChemPhotoChem* **2021**, *5*, 1042–1058.
[3] J. Wang, X. Zhang, H. Jia, S. Wang, P. Du, *Acc. Chem. Res.* **2021**, *54*, 4178–4190.
[4] Y. Li, H. Kono, T. Maekawa, Y. Segawa, A. Yagi, K. Itami, *Acc. Mater. Res.* **2021**, *2*, 681–691.
[5] S. E. Lewis, *Chem. Soc. Rev.* **2015**, *44*, 2221–2304.
[6] K. Y. Cheung, Y. Segawa, K. Itami, *Chem. Eur. J.* **2020**, *26*, 14791–14801.
[7] R. Jasti, J. Bhattacharjee, J. B. Neaton, C. R. Bertozzi, *J. Am. Chem. Soc.* **2008**, *130*, 17646–17647.
[8] S. Yamago, Y. Watanabe, T. Iwamoto, *Angew. Chem. Int. Ed.* **2010**, *49*, 757–759; *Angew. Chem.* **2010**, *122*, 769–771.
[9] H. Takaba, H. Omachi, Y. Yamamoto, J. Bouffard, K. Itami, *Angew. Chem. Int. Ed.* **2009**, *48*, 6112–6116; *Angew. Chem.* **2009**, *121*, 6228–6232.
[10] H. Omachi, S. Matsuura, Y. Segawa, K. Itami, *Angew. Chem. Int. Ed.* **2010**, *49*, 10202–10205; *Angew. Chem.* **2010**, *122*, 10400–10403.
[11] K. Y. Cheung, K. Watanabe, Y. Segawa, K. Itami, *Nat. Chem.* **2021**, *13*, 255–259.
[12] T. Kawase, H. R. Darabi, M. Oda, *Angew. Chem. Int. Ed.* **1996**, *35*, 2664–2666; *Angew. Chem.* **1996**, *108*, 2803–2805.
[13] G. Povie, Y. Segawa, T. Nishihara, Y. Miyauchi, K. Itami, *Science* **2017**, *356*, 172–175.
[14] M. R. Shortreed, S. F. Swallen, Z.-Y. Shi, W. Tan, Z. Xu, C. Devadoss, J. S. Moore, R. Kopelman, *J. Phys. Chem. B* **1997**, *101*, 6318–6322.
[15] Z. Xu, J. S. Moore, *Angew. Chem. Int. Ed.* **1993**, *32*, 1354–1357; *Angew. Chem.* **1993**, *105*, 1394–1396.
[16] A. S. Shetty, J. Zhang, J. S. Moore, *J. Am. Chem. Soc.* **1996**, *118*, 1019–1027.
[17] S. Höger, S. Rosselli, A.-D. Ramminger, V. Enkelmann, *Org. Lett.* **2002**, *4*, 4269–4272.
[18] L. Shu, M. Müri, R. Krupke, M. Mayor, *Org. Biomol. Chem.* **2009**, *7*, 1081–1092.
[19] Y. Tobe, N. Utsumi, A. Nagano, K. Naemura, *Angew. Chem.* **1998**, *110*, 1347–1349; *Angew. Chem. Int. Ed.* **1998**, *37*, 1285–1287.
[20] M. Mayor, J.-M. Lehn, *J. Am. Chem. Soc.* **1999**, *121*, 11231–11232.
[21] L. Shu, M. Mayor, *Chem. Commun.* **2006**, 4134–4136.
[22] R. Kandre, A. D. Schlüter, *Macromol. Rapid Commun.* **2008**, *29*, 1661–1665.
[23] R. M. Kandre, F. Kutzner, H. Schlaad, A. D. Schlüter, *Macromol. Chem. Phys.* **2005**, *206*, 1610–1618.
[24] T. C. Lovell, C. E. Colwell, L. N. Zakharov, R. Jasti, *Chem. Sci.* **2019**, *10*, 3786–3790.
[25] H. Gregorius, M. Baumgarten, R. Renter, K. Müllen, N. Tyutyulkov, *Angew. Chem. Int. Ed.* **1992**, *31*, 1653–1655; *Angew. Chem.* **1992**, *104*, 1621–1623.
[26] M. Iyoda, J. Yamakawa, M. J. Rahman, *Angew. Chem. Int. Ed.* **2011**, *50*, 10522–10553; *Angew. Chem.* **2011**, *123*, 10708–10740.
[27] K. J. Weiland, A. Gallego, M. Mayor, *Eur. J. Org. Chem.* **2019**, *2019*, 3073–3085.
[28] M. Gon, Y. Morisaki, R. Sawada, Y. Chujo, *Chem. Eur. J.* **2016**, *22*, 2291–2298.
[29] M. Gon, Y. Morisaki, Y. Chujo, *Chem. Commun.* **2017**, *53*, 8304–8307.
[30] Y. Morisaki, R. Sawada, M. Gon, Y. Chujo, *Chem. Asian J.* **2016**, *11*, 2524–2527.
[31] Y. Wu, G. Zhuang, S. Cui, Y. Zhou, J. Wang, Q. Huang, P. Du, *Chem. Commun.* **2019**, *55*, 14617–14620.
[32] J. He, M. Yu, M. Pang, Y. Fan, Z. Lian, Y. Wang, W. Wang, Y. Liu, H. Jiang, *Chem. Eur. J.* **2022**, *28*, e202103832.
[33] K. J. Weiland, T. Brandl, K. Atz, A. Prescimone, D. Häussinger, T. Šolomek, M. Mayor, *J. Am. Chem. Soc.* **2019**, *141*, 2104–2110.
[34] M. Hasegawa, Y. Ishida, H. Sasaki, S. Ishioka, K. Usui, N. Hara, M. Kitahara, Y. Imai, Y. Mazaki, *Chem. Eur. J.* **2021**, *27*, 16225–16231.
[35] Y. Morisaki, K. Inoshita, Y. Chujo, *Chem. Eur. J.* **2014**, *20*, 8386–8390.
[36] Y. Morisaki, M. Gon, T. Sasamori, N. Tokitoh, Y. Chujo, *J. Am. Chem. Soc.* **2014**, *136*, 3350–3353.
[37] X. Li, A. Staykov, K. Yoshizawa, *BCSJ* **2012**, *85*, 181–188.
[38] K. Reznikova, C. Hsu, W. M. Schosser, A. Gallego, K. Beltako, F. Pauly, H. S. J. van der Zant, M. Mayor, *J. Am. Chem. Soc.* **2021**, *143*, 13944–13951.
[39] S. Castro-Fernández, R. Yang, A. P. García, I. L. Garzón, H. Xu, A. G. Petrovic, J. L. Alonso-Gómez, *Chem. Eur. J.* **2017**, *23*, 11747–11751.
[40] K. Zhu, K. Kamochi, T. Kodama, M. Tobisu, T. Amaya, *Chem. Sci.* **2020**, *11*, 9604–9610.
[41] G. Meyer-Eppler, R. Sure, A. Schneider, G. Schnakenburg, S. Grimme, A. Lützen, *J. Org. Chem.* **2014**, *79*, 6679–6687.
[42] Y. Segawa, S. Miyamoto, H. Omachi, S. Matsuura, P. Šenel, T. Sasamori, N. Tokitoh, K. Itami, *Angew. Chem. Int. Ed.* **2011**, *50*, 3244–3248; *Angew. Chem.* **2011**, *123*, 3302–3306.
[43] J. L. Alonso-Gómez, P. Rivera-Fuentes, N. Harada, N. Berova, F. Diederich, *Angew. Chem. Int. Ed.* **2009**, *48*, 5545–5548; *Angew. Chem.* **2009**, *121*, 5653–5656.
[44] C. Schaack, E. Sidler, N. Trapp, F. Diederich, *Chem. Eur. J.* **2017**, *23*, 14153–14157.
[45] J. Y. Xue, K. Ikemoto, N. Takahashi, T. Izumi, H. Taka, H. Kita, S. Sato, H. Isobe, *J. Org. Chem.* **2014**, *79*, 9735–9739.
[46] Z. Hassan, E. Spuling, D. M. Knoll, J. Lahann, S. Bräse, *Chem. Soc. Rev.* **2018**, *47*, 6947–6963.
[47] N. Berova, L. D. Bari, G. Pescitelli, *Chem. Soc. Rev.* **2007**, *36*, 914–931.
[48] J. Roose, S. Achermann, O. Dumele, F. Diederich, *Eur. J. Org. Chem.* **2013**, 3223–3231.
[49] G. Snatzke, *Angew. Chem.* **1979**, *91*, 380–393; *Angew. Chem. Int. Ed.* **1979**, *18*, 363–377.
[50] H. Hopf, I. Dix, *Synlett* **2006**, 1416–1418.

Manuscript received: June 8, 2022
Accepted manuscript online: July 4, 2022
Version of record online: August 3, 2022